Check for updates

JOURNAL OF FIRE SCIENCES

Original Research Article

Journal of Fire Sciences
2022, Vol. 40(1) 44–69
© The Author(s) 2021
Article reuse guidelines:
sagepub.com/journals-permissions
DOI: 10.1177/07349041211056343
journals.sagepub.com/home/jfs
SAGE

Mine conveyor belt fire classification

Manuel J Barros-Daza[1], Kray D Luxbacher[1], Brian Y Lattimer[2] and Jonathan L Hodges[3]

Date received: 29 June 2021; accepted: 12 October 2021

Abstract

This article presents a conveyor belt fire classification model that allows for the determination of the most effective firefighting strategy. In addition, the effect of belt design parameters on the fire classification was determined. A methodology that involves the use of numerical simulations and artificial neural networks was implemented. An approach previously proposed for modeling fires over conveyor belts was used. With the objective of obtaining some required modeling input parameter and verifying the capacity of this approach to get realistic results, computational fluid dynamics model calibration and validation were carried out using experimental test results available in the literature. Results indicated that scenarios with belt positions closer to the mine roof and greater tunnel heights require a higher longitudinal air velocity to be attacked directly. Furthermore, the belt fire classification model provided by the artificial neural network had an accuracy around 95% when test scenarios were classified.

Keywords

Mine fire classification, artificial neural network neural network, belt fires, critical velocity, mine firefighters

Introduction

After a fire is confirmed in a mine, personnel must be safely evacuated and the mine system brought back into balance by either containing or extinguishing the fire.[1,2] During mine fire response, two main decisions can be made: direct attack and indirect attack. Direct attack

[1]Department of Mining and Minerals Engineering, Virginia Tech, Blacksburg, VA, USA
[2]Department of Mechanical Engineering, Virginia Tech, Blacksburg, VA, USA
[3]Jensen Hughes, Blacksburg, VA, USA

Corresponding author:
Manuel J Barros-Daza, Department of Mining and Minerals Engineering, Virginia Tech, 117A Surge Building, 400 Stanger Street (MC 0239), Blacksburg, VA 24061, USA.
Email: manuel1@vt.edu

refers to a firefighting process involving the application of extinguishing agents directly onto the burning fuel.[3] Indirect attack refers to a fire suppression at a considerable distance away from the fire where it is not possible to apply agents onto the burning fuel since evacuation of the fire area or mine is required.[3] Indirect attack in underground coal mines generally involves sealing which refers to enclose the fire area or entire mine in order to exclude oxygen or flooding with water or gases such carbon dioxide and nitrogen.[4] It is noteworthy that the type of attack must be selected based on the fire characteristics and conditions at the fire proximity. Mine fires such as conveyor belt fires can grow rapidly and deteriorate the conditions very fast[5,6] in which a wrong decision will put at risk the mine personnel and could cause catastrophic consequences. Fire effects analysis prior to belt fire occurrence can provide insightful information allowing for the best decision that increases the probability to extinguish the fire without compromising the health and safety of the firefighting personnel.

If a belt fire cannot be extinguished within a short time after discovery using direct attack, the chance of safely controlling and extinguishing the fire quickly without evacuation and sealing is greatly reduced.[2] The selection of direct attack seems to be the best decision regarding time, cost, and mine productivity; however, direct extinguishing must be selected and carried out as long as the health and safety of the firefighting personnel are not compromised.[7] Title 30 CFR § 75.1502 (a) requires that each underground coal mine operator adopts and follows a firefighting program which instructs all miners in the proper procedures to follow in case of a mine emergency.[8] Nevertheless, these procedures leave some space for subjective decisions that could lead to risky situations due to the extreme conditions produced by the fire.

In order to analyze fire effects prior to their occurrence, computational fluid dynamics (CFD) modeling has been used to reduce the number of large-scale experiments. Once CFD models are calibrated or validated, they can provide useful information related to flame spread rate, fire size, amount of smoke, and toxic gases produced.[9] Yuan et al.[10] carried out a CFD model calibration and validation of a fire spreading over a conveyor belt in a mine entry based on results of a large-scale experimental test. The CFD model was in good agreement with experimental results in some fire characteristics such as flame spread rate, the maximum fire heat release rate (HRR), downstream maximum smoke temperature, and maximum CO concentration at the exit. This study evidenced that Fire Dynamic Simulator (FDS) software can be used as a tool to predict the effects of fires spreading over a conveyor belt in a mine entry under different physical conditions. In the same way, Edwards and Hwang[11] used FDS to model fire spread along ribs, roof, timber sets, and over a conveyor belt in a coal mine entry. Results obtained from the CFD model overestimated the flame spread rate over the conveyor belt when they were compared with experimental data. This fact can be attributed to the lack of CFD model calibration with experimental data.[10] Similarly, Lowndes et al.[12] built a computational model in the three-dimensional (3D) CFD software Fluent to characterize the initiation and spread of fire along surfaces of a conveyor belt mounted within a ventilated full-scale experimental test gallery. Numerical results showed a good capacity to qualitatively replicate the flame spread observed on the belt surfaces within the test gallery.

Even though CFD modeling techniques have expanded successfully in the recent years reducing the number of experimental tests, these tests will always be important for validation and calibration purposes. Multiple large-scale experiments studying fire spreading over conveyor belts have been carried out and reported in the literature. Lazzara and Perzak[13] conducted a test in a large-scale fire gallery in order to measure the flame front velocity as

function of the imposed convective air velocity for a type of styrene-butadiene rubber (SBR). Results showed that the measured flame front velocity peaked at an air velocity equal to 1.5 m/s. Using the same fire gallery, Litton et al.[5] presented two nomographs defining sensor alarm levels and sensor spacing as a function of belt entry air velocity and belt entry cross-sectional area. Subsequently, Perera and Litton[6] used the nomographs to understand and quantify the effects of air velocity on the detection of fires in underground conveyor belt haulageways. Another large-scale experimental test with the objective of determining the flame spread rate on an SBR belt was carried out by Rowland and Smith.[14] They tested different air velocities from 1.0 to 4.0 m/s determining the highest spread rate of 7.41 cm/s for an air velocity of 2.0 m/s.

Haghighat and Luxbacher[15] carried out a tenability analysis for mine firefighters in underground coal fire scenarios. The authors examined the impact of a simulated methane fire at a continuous miner working face on conditions such as temperature, visibility, radiation, and toxicity. Several permutations of numerical simulations studying the impact of damage on ventilation controls were used to examine the risk to fire responders. The authors recommended tenable limits for different responders based on their equipment (i.e. bare-faced miners, mine rescue team, and the fire brigade). This previous research showed the numerical models were able to provide valuable insights into the tenability within a mine fire. However, this study focused on a miner face fire rather than a conveyor belt fire. In addition, prior studies have been limited to a limited set of simulations, with no attempts made to provide general support for real-time decision-making for emergency responders.

However, artificial neural network (ANN) is a machine learning technique widely used for classification problems in recent years. ANNs have been used in wildfire classification for fire detection, risk assessment, and recognition of high potential area for fire occurrence due to its ability to solve no-parametric, non-linear, large-scale, and very complicated models.[16] Researchers have recently used machine learning to approximate the detailed thermal flow field encountered in a mine fire.[17] This study showed the strength of ANNs to predict the conditions in a mine. However, this study did not focus on any specific mine fire scenario (i.e. miner face or conveyor belt). In addition, the researchers did not provide general support for real-time decision-making for emergency responders. A new machine learning–based model which is able to provide decision-making support for emergency responders would greatly improve fire risk analysis in a mine fire.

The objective of this study was to develop a conveyor belt fire classification model that allows for the determination of the most effective firefighting strategy, as well as the influence of belt design parameters on the fire classification. Parameters such as belt position, tunnel height, and width were studied and considered for the elaboration of the classification model. In order to achieve these objectives, a methodology that involves numerical simulation and a machine learning tool such as ANN was used. CFD simulations were used to study the effects produced by fires spreading over conveyor belts following the approach proposed by Yuan et al.[10] CFD model calibration was carried out using experimental test results available to obtain some required input parameters and verify the capacity of this approach to get realistic results. Different ANNs were used for the determination of parameter effects and the belt fire classification model. Finally, it is worth saying that the methodology used in this study can be applied for classification of other mine fire types, such as working face fires and intake entry fires as well as the determination of models for critical velocity and response time in belt fire scenarios.

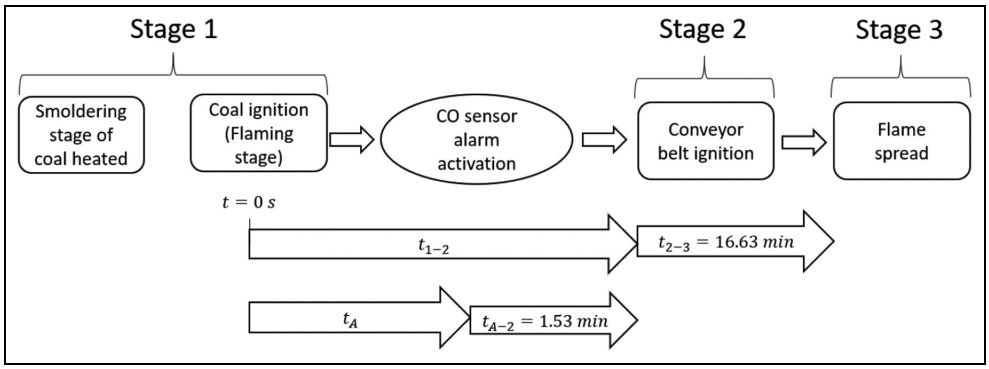

Figure 1. Conveyor belt fire stages in underground coal mines. Average times of CO alarm activation before the belt ignition and between Stages 2 and 3 were determined based on results reported by Perera and Litton[6] and Litton et al.,[5] respectively.

Conveyor belt fire stages and detection times

Fires occurring in conveyor belt entries generally progress in three different stages as shown in Figure 1. The first stage is related to a low-temperature smoldering combustion of coal. Loose coal is deposited along the belt drive area such as conveyor idlers or electrical cables where due to either frictional overheating or an electrical fault, coal is heated triggering a smoldering combustion. Once coal temperature goes up, coal ignites, and flames appear. The second stage starts when the conveyor belt is stopped, and the heat produced by the coal fire is enough to ignite the conveyor belt. Finally, in the third stage, the combined effect of coal and conveyor belt fires elevates the total fire intensity to the point of sustained belt flame spread.[5,6] It is important to point out that the fire detection should occur as soon as possible in order to secure the safety of underground workers and firefighting personnel as well as to increase the probability of successfully controlling and extinguishing the fire. Title 30 CFR § 75.350 requires mine operators to monitor for carbon monoxide thorough CO sensors. Such CO sensors must be installed at intervals not exceeding 300 m along each belt entry.[8]

In order to have a certain degree of understanding of the total time that firefighters have to approach the belt fire once it is detected, results of two previous experimental studies were used. These studies focused on belt fire detection time and time elapsed between fire stages. The first study was performed by Perera and Litton[6] that consisted of a large-scale experiment in which a conveyor belt composed of SBR material was used. In this study, the time elapsed between Stages 1 and 2 (t_{1-2}), roof CO alarm activation time (t_A), and the subtraction of these two times (t_{A-2}) for three different air velocities were reported as shown in Table 1. Times were referenced from Stage 1 when coal ignites ($t = 0$ s). Thus, negative time values in column 4 represent that the fire detection was achieved before belt ignition. On average, results show that CO alarms are activated 1.53 min before the belt ignition. During the experimental test, sensors were spaced 300 m as required by the mining regulation, and fire was assumed to be 150 m away from each sensor. In the second study carried out by Litton et al.,[5] the time elapsed between Stages 2 and 3 (t_{2-3}) reported for different air

Table 1. Results of belt ignition times and CO detection times for an SBR conveyor belt reported by Perera and Litton.[6]

Air velocity (m/s)	t_{1-2} (min)	t_A (min)	t_{A-2} (min)
1.0	3.8	1.7	−2.1
2.0	15	16	1.0
4.1	7.8	4.3	−3.5

Table 2. Times elapsed between Stages 2 and 3 reported by Litton et al.[5]

Air velocity (m/s)	t_{2-3} (min)
0.76	15.5
1.52	18.5
1.52	17.0
4.06	15.5

velocities as shown in Table 2. The average time elapsed between Stages 2 and 3 was estimated to be 16.63 min.

The extension of conveyor belts along underground coal mine entries is regularly in the order of tens of kilometers. For this reason, when belt fires occur in remote locations where there are no personnel around, firefighter deployment times are regularly greater than the time elapsed until the onset of the flame spread (around 18.16 min on average). Following a conservative approach and knowing that conditions can become untenable rapidly during belt fires, in this study, it was strongly recommended remote attack in scenarios that result inadequate for direct firefighting after the onset of the flame spread. This turns out that if conditions remain tenable for firefighters after flame spread, direct attack must be carried out.

Modeling the SBR

The modeling of flame spread over a conveyor belt is not an easy task since involves a complex interaction of highly non-linear phenomena. Flame spread over a conveyor belt is a process that involves gas phase turbulent flow, heat transfer between the flame, belt surface and surroundings surfaces, the vaporization of the belt material through the solid phase (pyrolysis reaction), and the chemical reaction of the gaseous fuel with the oxygen in the air. In addition, not all parameters related to materials involved in the pyrolysis process required for modeling are known.[9–11] Despite the complexity and limitations in flame spread modeling, Yuan et al.[10] proposed a simplistic approach for modeling flame spread over a conveyor belt using CFD technique. This approach overlooks underlying physics and the complexity of the fire spread phenomenon that could lead to not resolving the flame completely; however, numerical results of parameters needed in mine fire planning obtained from this approach have exhibited good agreement with experimental results as shown in Yuan et al.[10] and this work.

Following Yuan et al.'s[10] approach, FDS version 6.6 software was used to predict the effects produced by conveyor belt fires in different scenarios. FDS is a 3D, large-eddy simulation model used for studying the evolution of fire, transport of gases, and smoke in enclosed spaces. FDS solves the governing equations using second-order accurate finite differences on a collection of uniformly spaced 3D grids.[18] FDS is the most widely used large-eddy simulation model in the fire science field since it has demonstrated good agreement with experimental results in validation studies.[9]

The program models flame spread using a pyrolysis model alongside a gas phase combustion model. The pyrolysis model is in charge to simulate the decomposition of the belt material into the gas phase produced by a heat source. Then, the combustion model simulates the reaction between the gas phase and oxygen.[9] The pyrolysis and combustion processes are interdependent since the solid decomposition into the gas phase is produced by the heat transfer from the flame to the solid surface.

In order to model the pyrolysis process, FDS uses equation (1) that represents the conversion rate of any multicomponent material (1) to a gas during the pyrolysis reaction. It is noteworthy that equation (1) is valid as long as other materials do not produce material (i), and the residue and the reaction rate are not affected by the local oxygen volume fraction

$$\frac{dY_S}{dt} = -\sum_{j=1}^{N_{r,i}} r_{i,j} \tag{1}$$

In the above equation

$$r_{i,j} = A_{i,j} Y_{S,i}^{n_{S,ij}} \exp\left(-\frac{E_{i,j}}{RT_S}\right) \tag{2}$$

where $Y_S = \rho_{S,i}/\rho_o(0)$ is the normalized density of the solid fuel, $r_{i,j}$ defines the rate of reaction of the ith material undergoing its jth reaction at the temperature T_S, $E_{i,j}$ is the reaction at the temperature T_S, E_{ij} is the activation energy (kJ/mol), R is the gas constant (J/mol K), T is the temperature in which the reaction jth occurs (K), $n_{S,ij}$ is the reaction order, and $A_{i,j}$ is the pre-exponential factor (s^{-1}).

For a single material component, equations (1) and (2) can be simplified into equations (3) and (4), respectively

$$\frac{dY_S}{dt} = -r_{1,1} \tag{3}$$

$$r_{i,j} = A_{1,1} Y_{S,i}^{n_{S,1,1}} \exp\left(-\frac{E_{1,1}}{RT_S}\right) \tag{4}$$

As shown previously, to simulate the decomposition of the material, it is necessary to know the kinetic parameters such as pre-exponential factor (A) and the activation energy (E) associated with the pyrolysis. However, these parameters just mentioned are not easy to find or are unavailable for most of real materials.[9] Nevertheless, FDS can derive these values knowing the reference temperature (T_p) and the reference rate (r_p) through equations (5) and (6) for a single material with a single component. Thermogravimetric analysis (TGA) is commonly used to obtain these two parameters in which the reference temperature is defined

as the "temperature at which the mass loss rate curve from a TGA test peaks," and the reference rate is defined as "the value of peak mass loss rate"[9]

$$E_{1,1} = \frac{er_p RT_P^2}{\beta} \tag{5}$$

$$A_{1,1} = er_p e^{\frac{E}{RT_p}} \tag{6}$$

In this study, it was assumed that the conveyor belt is made of SBR since it is a polymer widely used for the fabrication of conveyor belts in the mining industry providing excellent abrasion and heat resistance.[19] According to TGA results published by Yuan et al.[10] and Grieco et al.,[20] SBR is a material with multiple components. Yuan et al.[10] observed in TGA results that SBR is made up of two components. A first component associated with a first peak evidenced at 232°C and reference rate equal to 0.0058 s^{-1}. This peak was elongated and narrow, and it represented the mass loss rate from 97% to 89%. The second peak, associated with the second component, was seen at 469°C and reference rate of 0.0022 s^{-1}. This second peak was wider and shorter than the first peak and represented the mass loss rate from 80% to 40%. However, Lin and Chang,[21] in a study carried out using rubber waste composed of SBR, reported three components. The first, second, and third peaks associated with each component were evidenced at 307°C, 447°C, and 597°C, respectively. However, Lin and Chang[21] concluded that the fraction of volatile matter produced by the third component is less than 15%. As can be seen in these TGA studies, the contribution for volatile matter production can be attributed to mainly the two first components with reference temperature around 250°C and around 450°C. Although main variables such as reference rate and reference temperature for the two main components of SBR are known properties, respective pyrolysis residues are difficult to obtain.[10] For this reason, Yuan et al.'s[10] approach proposed and demonstrated that SBR can be modeled as single component material in which only a reference temperature and reference rate are needed. Under this premise, it is assumed that SBR has a unique peak in the TGA analysis. This peak is expected to be between the first and second peaks associated with the components reported in the two studies mentioned previously.

In order to determine the reference temperature and the reference rate for the assumed single component of SBR, the model calibration was performed. The kinetic parameters were obtained by matching flame spread rates in both simulation and experimental results available in the literature during the calibration. Different reference temperatures (between 232°C and 469°C) and reference rates (between 0.0022 and 0.0058 s^{-1}) inside the interval of the peaks of the first two components mentioned previously were tested. A heating rate equal to 20 C/min used in the TGA analysis carried out by Yuan et al.[10] was set as input for the pyrolysis model.

The heat of combustion and gasification of the SBR used for the numerical simulations was 28,500 and 1500 kJ/kg, respectively. These values correspond to the fire-resistant SBR belt reported by Tewarson.[22] The heat of combustion for pure propylene is 48,902 kJ/kg, as reported by Wiberg and Fenoglio.[23] In order to avoid discrepancy with the SBR heat of combustion, FDS adjusts the mass loss rate of fuel gas to produce the expected HRR. Nevertheless, the mass of SBR is reduced according to the value of parameters established in the pyrolysis model.[9]

Table 3. Mole fractions of volatile matter composition during pyrolysis of SBR.[20]

Name	Formula	Mole fraction (%)
Carbon dioxide	CO_2	2.578
Ethylene	C_2H_4	17.138
Ethane	C_2H_6	7.623
Propylene	C_3H_6	26.26
Propane	C_3H_8	10.371
Hydrogen	H_2	17.205
Methane	CH_4	18.825
Carbon monoxide	CO	18.825

The percentages of volatile matter and char material produced during the pyrolysis process were set to 63% and 37% based on the values reported by Grieco et al.,[20] respectively. Also, in the same study, the components of volatile matter produced during pyrolysis of SBR were reported. This composition is shown in Table 3, in which the gas mixture is composed of seven different gases. The percentage of molar fraction for each gas is also showed in Table 3. However, it is important to mention that in FDS only one gaseous fuel can be in the combustion reaction. McGrattan et al.[9] recommend using the most predominant burn gaseous fuel. Thus, propylene was the gas selected.

For the determination of some of the tenability parameters discussed in a following section, the post-combustion yields of CO (Y_{CO}) and soot (Y_{soot}) were determined. Y_{CO} and Y_{soot} are defined as the fraction of fuel mass converted into carbon monoxide and smoke particulate, respectively. These values are reported in the literature based on the mass of SBR material burned. Thus, considering the heat of combustions of SBR and propylene, only a fraction of 0.58 of the expected amounts of CO and soot are really released during simulations, since in FDS, the mass loss rate of fuel gas is adjusted to produce the expected HRR.[9] In order to make up for the reduced production of CO and soot, and follow a conservative approach, upper limits of ranges of these parameters proposed in the literature were selected. The amount of carbon monoxide produced during the combustion of SBR increases as a function of the equivalence ratio (ϕ) according to equation (7).[24] Yuan and Litton[25] concluded that flame spread typically occurred for $\phi>1$ (fuel-rich combustion). Thus, a conservative value for CO yield (Y_{CO}) was set to 0.12 for ϕ equal to 1.25. The value of soot yield (Y_{CO}) produced during a fire of an SBR tire was reported within a range of 0.03 and 0.11.[26] For this study, a soot yield of 0.11 was considered following a conservative approach for firefighters. A summary of properties of SBR and charring material used in the numerical simulations are shown in Table 4[22,27]

$$Y_{CO} = 0.072\left(1 + 2.5exp\left(-2.5\phi^{-2.8}\right)\right) \tag{7}$$

Numerical details for model calibration and validation

Two different CFD domains (A and B) of conveyor belt entries were built to calibrate and validate the CFD model, respectively. As mentioned previously, model calibration and validation were performed in this study to determine some required input parameters for modeling and verify the CFD model capacity of predicting realistic results.

Table 4. Properties of SBR and charring material used in numerical simulations.

Property	SBR	Charring
Density (kg/m^3)	1300[27]	600[27]
Specific heat (kJ/kg K)	1.3[27]	0.6[27]
Conductivity (W/m K)	0.19[27]	0.09[27]
Heat of combustion (kJ/kg)	28,500[22]	–
Heat of gasification (kJ/kg)	1500[22]	–
Volatile matter (%)	63[20]	–
Char material (%)	–	37[20]
Y_{CO}	0.12[24,25]	–
Y_{soot}	0.11[26]	–

SBR: styrene-butadiene rubber.

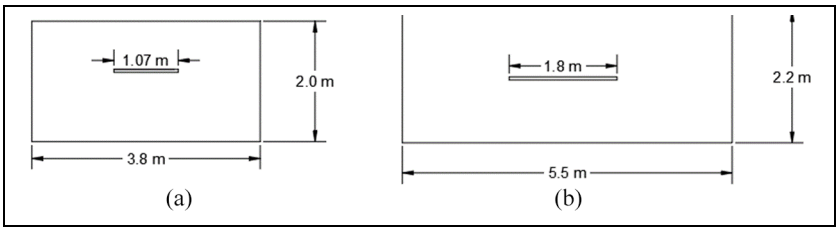

Figure 2. Cross-section of (a) Domain A and (b) Domain B.

Figure 2(a) shows the cross-section of CFD Domain A that was used for model calibration and built based on the geometry of the fire tunnel used by Lazzara and Perzak.[13] In this experimental test, flame spread rate was measured for different air velocities. Although the cross-sectional area of the CFD domain and tunnel were the same 7.6 m^2, the cross-sectional shapes were slightly different, since in FDS, it is not possible to have non-rectangular geometries.[9] CFD Domain A was 2.0 m high and 3.8 m wide. The conveyor belt was in the center of the mine entry 1.4 m off the right and left walls. Thermocouples were spaced 1.0 m apart from each other on the belt surface in order to determine the flame position over time as well as the flame spread rate for different air velocities. The flame position was determined where the belt surface reached 391°C. This temperature was reported as the piloted ignition temperature for the SBR belt meaning that SBR breaks down to volatile fuel at a rate enough to maintain a flammable mixture.[27]

The CFD Domain B shown in Figure 2(b) was used for model validation and built based on the tunnel in which the experimental test of Yuan et al.[10] was carried out. CFD Domain B was used to determine the fire HRR and belt surface temperatures in order to be compared with the experimental and numerical results reported by Yuan et al.[10] CFD Domain B was 2.2 m high and 5.5 m wide. The conveyor belt was located at the center of the mine entry 1.85 m away from the right and left walls. The mean air velocity was set to 1.5 m/s as used in the experiment.

Virtual heater elements were located close to the conveyor belt in order to simulate hot spots that trigger the decomposition of the belt material in both CFD domains. For the

numerical simulation, an ignition source is not needed, since FDS assumes that once the fuel gas and the oxygen are in contact, the combustion reaction starts.[9] The virtual heaters were set at 1600°C, providing around 7.0 kW each, since the ignition heat for SBR was estimated around 14 kW.[25] Virtual heaters were maintained turned on during the flame spread since they were used to simulate the coal fire that usually ignites the conveyor belt and remains active during this process. The belt conveyor was located 4.0 m from the tunnel inlet with a belt thickness of 15 mm.

Grid analysis, model calibration, and validation

During model calibration, different reference rates (between 0.0022 and 0.0058 s^{-1}) and reference temperatures (between 232°C and 469°C) were used. Model calibration was stopped once the mean of absolute error for model flame spread predictions calculated using equation (8) was lower than 0.5 cm/s. Experimental results reported by Lazzara and Perzak[13] were used for the calculation of this error. A grid size of 0.1 m was used since Yuan et al.[10] reported good agreement when this grid was used to simulate flame spread over conveyor belts. The lowest average absolute error equal to 0.47 cm/s was obtained for a reference rate equal to 0.0022 s^{-1} and reference temperature equal to 368°C. Figure 3 shows the flame spread rate for different air velocities obtained from model using the 0.1-m grid and reported by Lazzara and Perzak.[13] It can be seen that numerical values obtained using this grid size and experimental values are in good agreement for the range of velocity between 0.8 and 4.1 m/s. The model can reproduce the behavior of the flame spread rate peaking at 1.5 m/s and then decreasing for greater air velocities. Despite the good agreement between numerical and experimental results using a 0.1-m grid, flame spread rate was also calculated using a finer grid equal to 0.05 m. This was performed to evaluate if the proximity between results was an instance where the modeling uncertainties canceled out since it was considered a 0.1-m grid relatively coarse to reproduce the flame adequately. Furthermore, as the objective of this article was to predict fire conditions upwind from the fire, HRR (a variable with high influence on fire conditions), visibility, and temperature were also calculated using both grids in Domain A for scenarios with air velocities between 1 and 3 m/s. This velocity range was the one used to develop the conveyor belt fire classification model as shown in a following section

$$E_{Param,g} = \left| Param_{exp} - Param_{model,g} \right| \tag{8}$$

where $E_{Param,g}$ is the absolute error for parameter prediction using a grid size g, $Param_{exp}$ is the value of the parameter reported in the experimental test, and $Param_{model,g}$ is the value of the parameter predicted by the model using a grid size g.

Flame spread results obtained using the fine grid are shown in Figure 3. Figure 4 shows the HRR, visibility, and temperature using both grids for scenarios with air velocity equal to 1.5, 2.0, and 2.5 m/s. The results of visibility and temperature were calculated at an attack position 3 m away from the fire and at height 1.5 m from the floor. The mean of absolute error for model flame spread predictions calculated using equation (8) for both grids ($\overline{E}_{FSR,Coarse}$ and $\overline{E}_{FSR,Fine}$) is shown in Table 5. The mean of percent error of the maximum HRR ($\overline{PE}_{HRR}$) and temperature ($\overline{PE}_{Temp}$), and the minimum value of visibility ($\overline{PE}_{Vis}$) predicted by the model using the coarse grid when compared with predictions using the fine

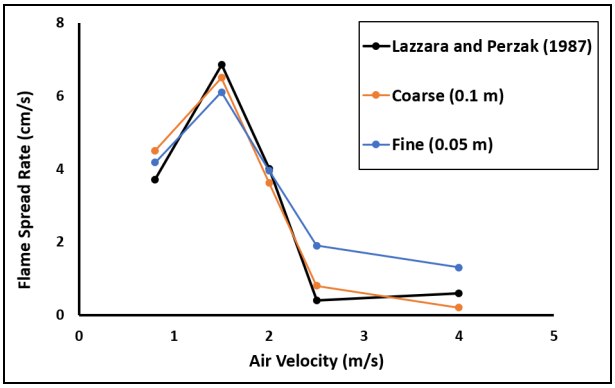

Figure 3. Comparison of flame spread rate for different air velocities determined by the calibrated model using the coarse and fine grids in Domain A, and Lazzara and Perzak[13] in an experimental test.

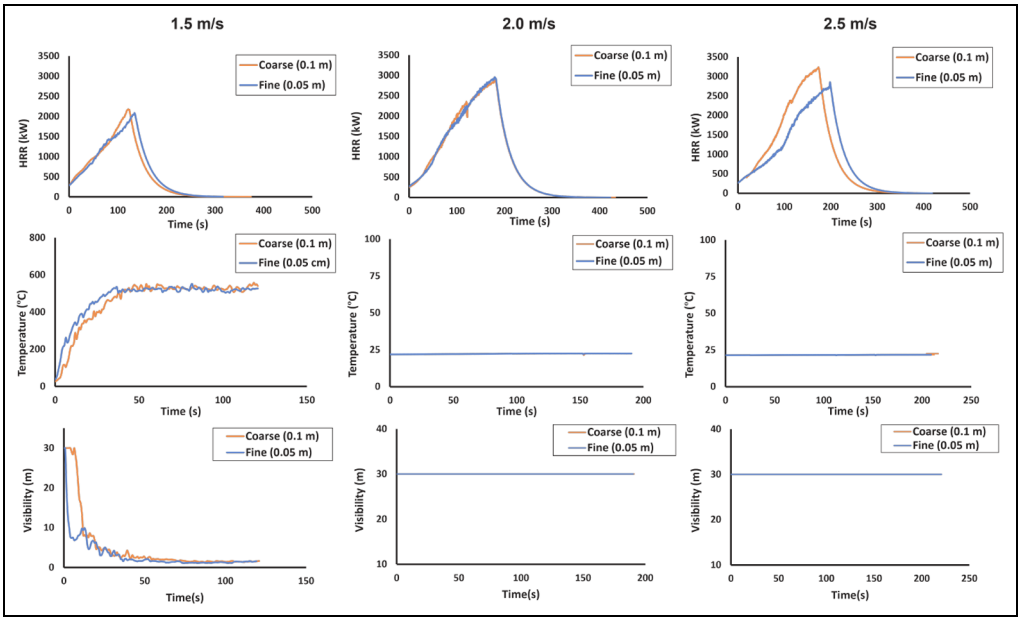

Figure 4. HRR, visibility, and temperature results using both grids in the CFD Domain A for different air velocities.

grid are shown in Table 5. Coarse grid error percent of the parameters mentioned were calculated using equation (9).

Two observations can be noticed from these grid analysis results. First, the mean of absolute error for model flame spread predictions was not reduced when the fine grid was used, indicating that the agreement between coarse grid simulation and test results could be an instance where the uncertainties are canceled out; however, flame spread rate behavior and

Table 5. Summary of results of grid analysis, model calibration, and validation.

Parameter	Value	Units
$\overline{E}_{FSR,\,Coarse}(calibration)$	0.47	cm/s
$\overline{E}_{FSR,\,Fine}$	0.79	cm/s
$\overline{PE}_{HRR}$	6.07	%
$\overline{PE}_{Temp}$	1.53	%
$\overline{PE}_{Vis}$	0	%
$\overline{PE}_{HRR}(validation)$	7.04	%

most of its values predicted were consistent with experimental results. Due to its approximation in the reproduction of flame spread phenomenon, this approach could be used for estimation of conditions during belt fires as also suggested by Yuan et al.[10] Second, HRR, temperature, and visibility percent error means were lower than 10% for the coarse grid when compared with results using the fine grid showing an acceptable convergence.

Considering that the objective of this article is not focused on resolving the flame spread to sufficient detail but predicting fire conditions, this approach with a grid size of 0.10 m and calibrated parameters is recommended to be used for fire condition predictions as long as it can be validated. This recommendation is based on the coarse grid percent error is lower than 10% and hundreds of simulations are required for any parametric study

$$PE_{Param} = \frac{\left|Param_{model,\,c} - Param_{model,\,f}\right|^{*}}{Param_{model,\,f}}\ 100 \tag{9}$$

where PE_{Param} is the percent error of parameter predicted by the model using the coarse mesh. $Param_{model,\,c}$ and $Param_{model,\,f}$ are the value of parameter predicted by the model using the coarse and fine grids, respectively.

In order to test the calibrated model capacity predicting fire conditions, a model validation was performed. A numerical simulation was performed in the CFD Domain B in order to compare numerical results with experimental values of the fire HRR and belt surface temperatures reported by Yuan et al.[10] The fire HRR evolution in the simulations and experiment after the onset of the flame spread is shown in Figure 5. The maximum HRR was around 7600 and 8000 kW in the experimental test reported by Yuan et al.[10] and models, respectively, and it was reached at 400 s after the beginning of flame spread. The percent error of the maximum HRR predicted by the model when compared with experimental results was 7.04% which indicated an acceptable agreement. However, FDS models seem to underestimate the HRR during the growth stage. In addition to the HRR, comparison of surface temperatures between test and model reported in Yuan et al.,[10] and results of the calibrated model was performed as shown in Figure 6. Figure 6 shows the belt surface temperatures at two positions from belt front. Simulation results of the calibrated model regarding the evolution of temperature at 6 m from the belt front show good agreement with experimental and Yuan model values. Nevertheless, some discrepancy can be seen at 3 m from the belt front with experimental values. Despite these discrepancies, the range of temperature values is the same.

Based on these results, it can be stated that the proximity between model predictions and experimental values allows to validate the calibrated model using a 0.1-m grid. Model

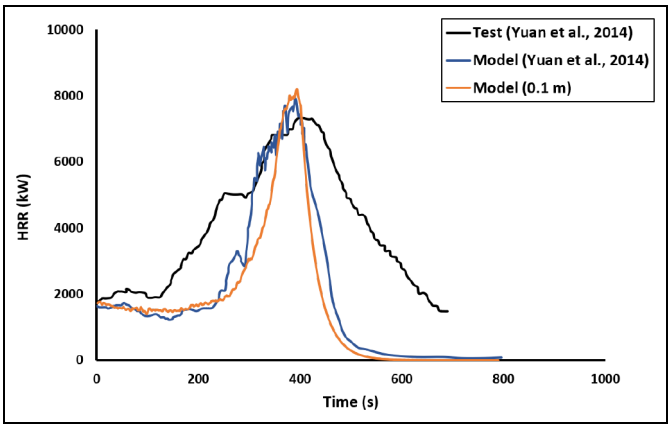

Figure 5. Comparison of heat release rate (HRR) between the calibrated model in Domain B and results reported by Yuan et al.[10]

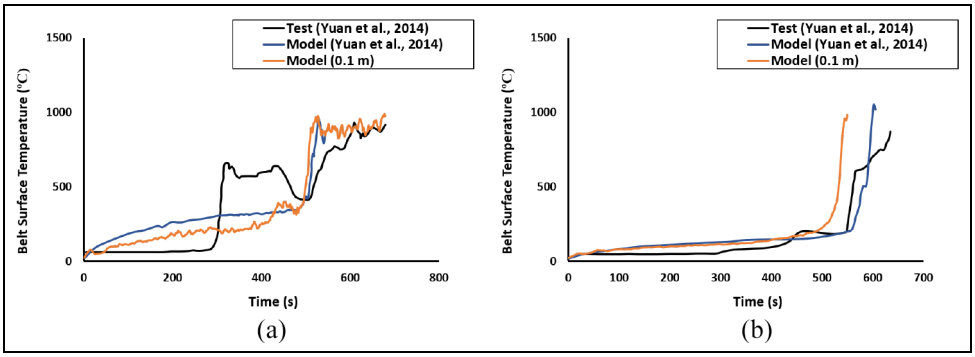

Figure 6. Comparison of surface temperatures between test and simulations: (a) 3 m from belt front and (b) 6 m from belt front.

validation is accepted since the main objective of this article is to determine fire conditions produced by the belt fires in which the HRR has the highest influence. However, it is noteworthy that the almost exact match between the calibration case using the coarse grid (0.1 m) and experimental results of flame spread rate could be an instance where the uncertainties are canceled out. This is demonstrated with the poor agreement between test and model in belt surface temperature at 3 m from belt front, the fire growth stage in the validation case (see Figure 5), and the results of flame spread using a finer grid. These facts indicate that the approach used has limitations reproducing the flame spread phenomenon due to the lack of physics in the model even though finer grid is used to resolve the flame more adequately. Thus, it is recommended to use this approach for prediction of fire conditions produced by flame spread over conveyor belts; however, more development is needed on this approach for studying flame spread over conveyor belts with certainty.

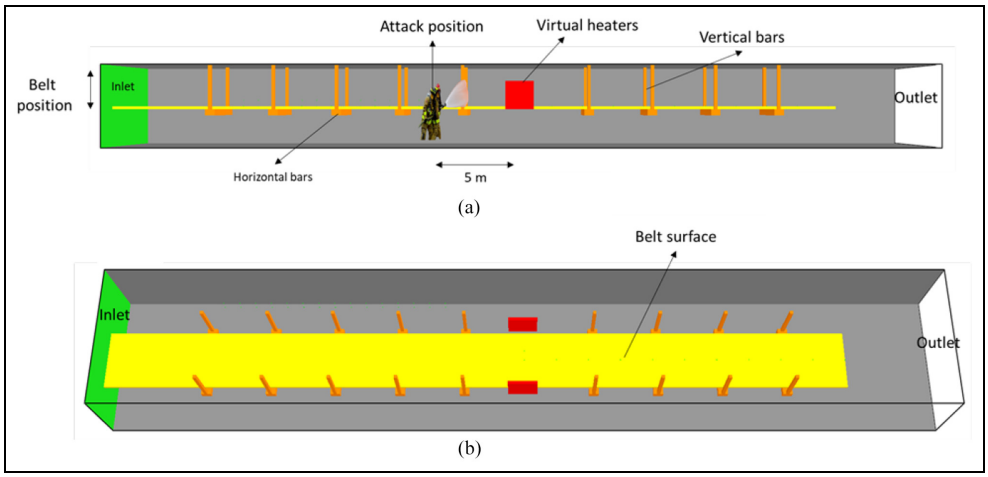

Figure 7. CFD domain of conveyor belt: (a) side view and (b) top view.

Conveyor belt fire model

A CFD domain similar to belt entries of partner mines as shown in Figure 7 was used to study the effects of fire spreading over conveyor belts on underground conditions. The domain's width and height were varied between 4.0 and 7.0 m and 1.8 and 2.8 m, respectively. The domain length of 26.0 m was maintained constant. The conveyor belt was located 1.0 m off the right wall. The conveyor belt surface was 23.0 m long, 1.8 m wide, and was composed of SBR. The kinetic parameters obtained during the calibration and properties of SBR shown in Table 4 were used in these numerical simulations. The walls were composed of coal with thickness of 0.10 m. The Pittsburg coal properties such as density, conductivity, specific heat, and emissivity were used and set to 1323 kg/m^3, 0.214 W/mK, 1.66 kJ/kg K, and 0.96, respectively.[28] The conveyor belt structure consisted of horizontal bars attached to vertical chains hooked to the roof as shown in Figure 7. Horizontal bars were 2.4 m long. The vertical chains and horizontal bars were spaced 2 m from each other. The chains and horizontal bars were assumed to be made of steel. Steel property values of 0.85, 8050 kg/m^3, 45.8 W/K, and 0.46 kJ/kg K were set as emissivity, density, conductivity and specific heat,[29] respectively. As in the simulations used for calibration, the fire was ignited by virtual heaters located next to the conveyor belt. Virtual heater dimensions were 0.9 m long and 0.9 m wide. They were also set to 1600°C during the flame spread.

According to the Title 30 CFR § 75.350 (b) (7), the minimum air velocity in the belt entry must be 0.5 m/s and must not exceed 5.0 m/s.[8] Previous studies have shown that air velocity and belt position contribute to the heat transfer along the mine entry, influencing the flame spread rate, HRR produced by the fire,[25,30] and consequently, the underground conditions. For this reason, air velocity was varied between 1.0 and 3.0 m/s and belt position between 0.5 and 1.5 m. Belt position is defined as the distance between the belt surface and the mine entry roof. The range of parameters varied in simulations is shown in Table 6.

Table 6. Parameters varied during scenarios for the determination of effects of belt fires on underground firefighters.

Parameters	Range
Air velocity (m/s)	1.0–3.0
Belt position (m)	0.5–1.5
Height (m)	1.8–2.8
Width (m)	4.0–7.0

Table 7. Description and recommendation for each type of fire.

Fire type	Description
Type I	Direct attack is recommended
Type II	Remote attack is recommended

Fire classes and exposure limits

Four parameters such as temperature, visibility, radiation, and toxicity are normally investigated during tenability analysis to determine the conditions for firefighting personnel.[15,31–33] In this study, scenarios in which conditions remain tenable for direct attack, and scenarios which human life cannot be supported and indirect attack is required were determined. A tenable environment refers to a location where none of the exposure limits have been exceeded. Thus, two different types of belt fires were proposed in this study as shown in Table 7.

Generally, in underground coal mining, firefighting activities are carried out by two groups. The first group is the first responder group composed of bare-faced personnel that works daily in the mine. The second group is the second responder group mainly composed by the fire brigade.[2] For this study, it was only considered the second responder group for the model elaboration and parameters analysis. It is noteworthy that the members of this group carry self-contained breathing apparatus (SBCA), have specialized firefighting tools, and wear fire-resistant clothing.[2] Thus, toxicity elements such as combustion gas concentrations (CO and CO_2) and oxygen (O_2) concentration were not accounted for them since they have breathing apparatus, and it has been demonstrated that exposure limit for temperature, radiation, and visibility is first exceeded than toxicity during fire scenarios.[15,32]

In the course of this study, all exposure limits were considered as ceiling limits in order to follow a conservative approach. As recommended by Haghighat and Luxbacher,[15] exposure limits for temperature and radiant heat were set to 100°C and 5.0 kW/m^2 for the second responder group, respectively. For purposes of this work, the ceiling limit for visibility was set to 5 m. It is noteworthy that visibility is the most subjective criteria; however, Gehandler et al.[32] proposed this visibility limit for firefighting personnel who knows the environment where the fire occurs. The visibility limit is usually determined based on the relationship between walking speed and visibility.[34] In FDS, the maximum visibility was set to 30 m and the optical coefficient (C) was set to 3, assuming light reflecting steel chains and reflecting signs hanging on belt entry walls. A summary of ceiling limits for the parameters used in this study is shown in Table 8.

Table 8. Ceiling limits for the different parameters.

Fire type	Description
Heat flux (kW/m^3)	<5.0[15]
Temperature (°C)	<100[15]
Visibility (m)	>5[32]

Table 9. ANN architectures.

Parameters	Hidden layers	Units in each hidden layer
Arch1	1	[1]
Arch2	1	[2]
Arch3	1	[4]
Arch4	1	[8]
Arch5	2	[2,2]
Arch6	2	[2,4]
Arch7	2	[4,4]

Neural networks

ANNs were used in this study to determine the effects of parameters on conditions at the attack position and elaborate the classification model. Each ANN used in this study was trained using stochastic gradient descent (SGD) solver. The maximum number of iterations allowed during training was 4000. The loss function used in training was cross-entropy. Logistic function was used as activation function for hidden layers. To determine the best architecture for each case, cross-validation (CV) and mean classification accuracy metric were used. Architectures tested for each ANN are shown in Table 9. All network structures were composed of one input layer, one output layer, and one or two hidden layers depending on the architecture. It is important to say that L2-norm regularization technique was used with an alpha parameter equal to 0.5 to avoid overfitting in the margins provided by ANNs for fire classification. For illustration purpose, architecture "Arch6" is shown in Figure 8 in which the first hidden layer was composed of two units and the second hidden layer was composed of four units. The number of units in the input layer can vary depending on the number of input parameters used as it will be showed in the following sections. Architectures were built using scikit-learn that is a free software machine learning library for the python programming language.[35]

Results and discussion

Four-hundred CFD scenarios were simulated to determine the conveyor belt fire classification model and effect of parameters such as air velocity, belt position, tunnel height, and width on the fire classification. The values of input parameters for each unique scenario were obtained using simple random sampling from uniform distributions. This means that each value within a range had the same probability of being chosen during the sampling process. For the determination of the fire type in each scenario, tenability parameters shown in Table

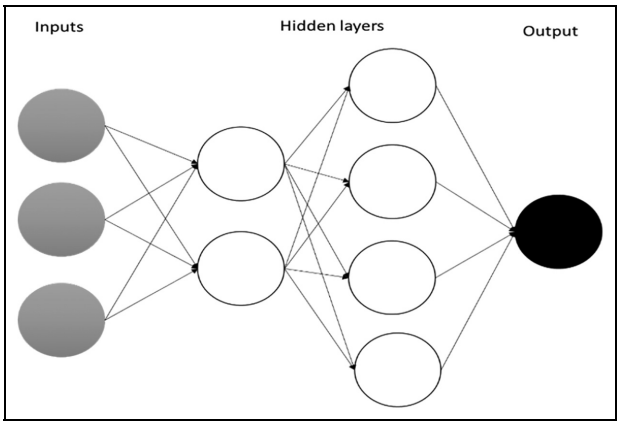

Figure 8. Arch6 architecture.

8 were calculated at an attack position 5 m upwind from the fire at intervals of 1 s during 900 s. As mentioned by Mcpherson,[36] the attack position for underground coal mine fires can be up to 10 m away from the fire, and it is totally dependent on the mine entry height. For this study, an attack position of 5 m upwind from the fire seems reasonably for the range of tunnel heights simulated. However, it was considered that firefighting personnel would try to crouch when they approach and attack the fire with the objective to stay below the smoke layer as also was assumed by Haghighat and Luxbacher.[15] Thus, tenability parameters were determined at a height of 1.5 m from the floor.

Simulation results were compared with the tenability limits allowing for the fire classification of each scenario as shown in Figure 9. In Figure 9 graphs, each point represents a scenario in which green triangles correspond to fire Type I and orange dots correspond to scenarios classified as Type II. In these graphics, air velocity was plotted along x-axis and compared with the other three parameters since it is the variable with the highest influence on the fire classification as discussed later. Most of Type I and Type II fires are located on the right and left sides of the plots, respectively. However, more overlapping between fires Type I and Type II at the center of the plot can be seen when tunnel width was plotted, indicating a possible negligible influence on the fire classification. In order to determine the influence of the four parameters on the fire classification, seven ANNs were used. The first four ANNs were utilized to determine the influence of each parameter individually. Subsequent, the second three ANNs were implemented to determine the effects of parameters when combined with air velocity. After all, a final ANN was implemented in which the input parameters were the ones with the highest influence on the fire classification allowing for the determination of the conveyor belt fire classification model.

In order to determine the effect of parameters on fire classification, ANNs were training using the entire data set. As mentioned previously, different architectures were evaluated. The architecture with the highest CV accuracy was selected in each case. The methodology used for determining the effect of parameters on fire classification is shown in Figure 10. In this methodology, threefold CV was carried out in order to select the best architecture. Once the architecture was selected, the ANN was trained to determine accuracy and the classification margin allowing for the determination of parameters effect on fire classification.

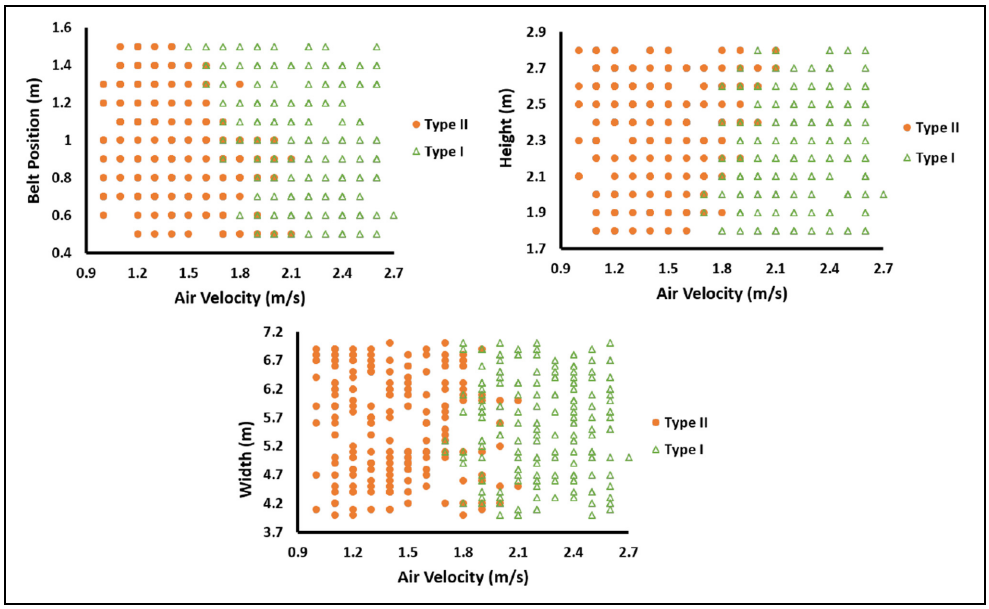

Figure 9. Classification of fire scenarios with respect to design parameters.

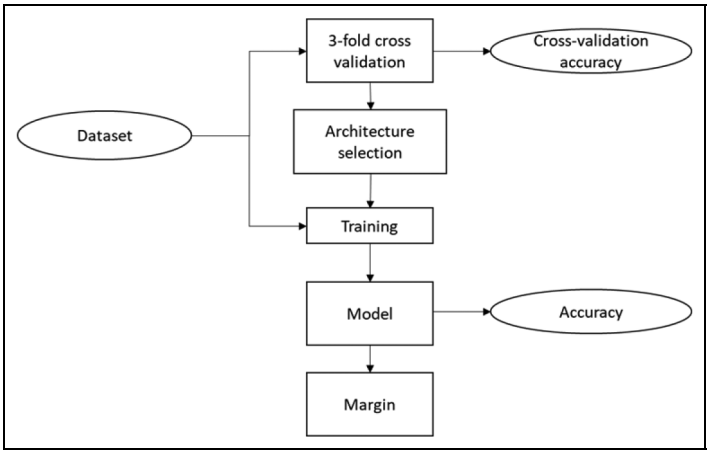

Figure 10. Methodology for the determination of the best model, training, and validation accuracies for each ANN.

Air velocity was used as an input parameter in ANN-00. The highest CV accuracy of 88.73% was obtained for Arch1 and an accuracy of 89.00% was obtained for the entire data set as shown in Table 10. This indicates that only using air velocity as the input parameter, ANN-00 was able to classify 356 out of 400 samples correctly suggesting that air velocity can explain around 89% of the variability on fire classification. An architecture with a single

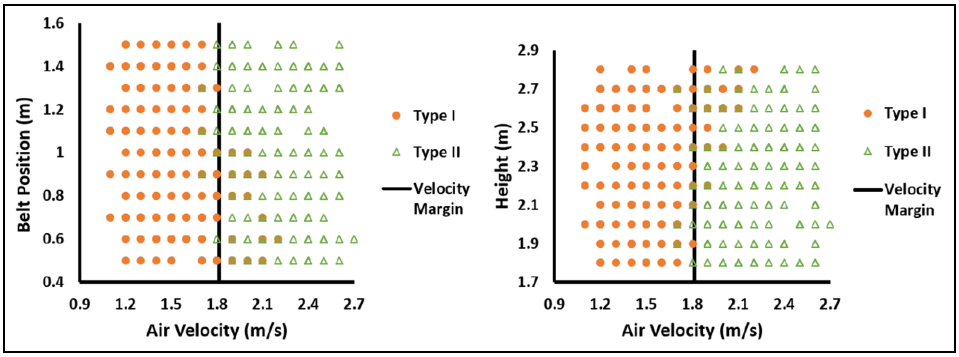

Figure 11. Velocity margin provided by ANN-00.

input parameter indicates that a value of velocity is determined by ANN-00 to separate fires Types I and II. To find this velocity value, 1000 velocities within the velocity range of scenarios used for training were fed into ANN-00. Then, the probability of each velocity of being Types I and II was determined. The velocity with probability equal to 0.5 of being both fire types was determined as the dividing point between fire Types I and II. This dividing point was determined to be located at 1.81 m/s. A margin equal to this velocity in two-dimensional (2D) plots is shown in Figure 11. Based on Figure 11, the critical velocity of a belt fire can be estimated to be between 1.5 and 2.2 m/s for the scenarios simulated in this article. Scenarios classified Type II within this critical velocity range exhibited fire sizes around 8000 kW. Applying the Thomas correlation shown in equation (10)[37,38] with the Froude number equal to 4.5 as proposed by Danziger and Kenned[39] the critical velocity was calculated to be around 1.6 m/s which indicates the proximity between results obtained in this study and Thomas[37,38] approach. However, some discrepancies can exist since the effect of the belt structure is not considered in the empirical correlation

$$V_c = \left[\frac{gQ}{\rho_o C_P \left(\frac{Q}{\rho_o C_p H V_c} + T_o W \right) A Fr_c} \right]^{\frac{1}{3}} \tag{10}$$

In the above equation, Q is the HRR of the fire (kW), V_c is the critical velocity (m/s), ρ_o is the ambient density (kg/m^3), C_p is the air specific heat (kJ/kg K), T_o is the ambient temperature (K), W is the tunnel width (m), A is the cross-sectional area of the tunnel (m^2), and Fr_c is the critical Froude number.

Belt position, tunnel height, and tunnel width were also used as individual input parameters for ANN-01, ANN-02, and ANN-03, respectively. As shown in Table 10, the accuracies for these three ANNs were 57.03%, 60.87%, and 51.15%, respectively. These values of accuracies reflect that these parameters by itself have a negligible influence on the fire classification. However, a synergistic effect could occur when they are combined with air velocity. For this reason, to determine the effects of each parameter when combined with air velocity, ANN-1, ANN-2, and ANN-3 were used. As shown in Table 10, the accuracies for ANN-1 and ANN-2 improved in comparison with ANN-00. However, similar accuracies between ANN-00 and ANN-3 were obtained indicating insignificant influence of tunnel width on the

Table 10. Networks' architecture and accuracy.

Name	Input parameters	Architecture	CV accuracy (%)	Accuracy (%)
ANN-00	Velocity	Arch1	88.73	89.00
ANN-01	Belt position	Arch1	58.57	57.03
ANN-02	Height	Arch2	61.64	60.87
ANN-03	Width	Arch2	57.06	51.15
ANN-1	Velocity, belt position	Arch6	92.32	92.07
ANN-2	Velocity, height	Arch6	92.08	92.07
ANN-3	Velocity, width	Arch7	88.24	88.50

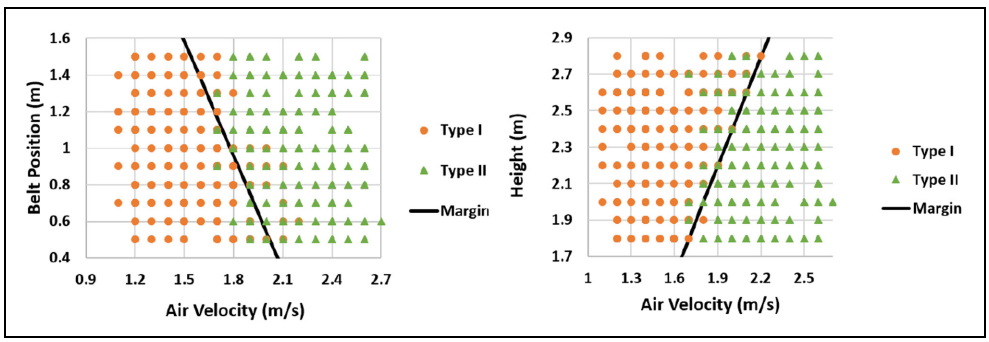

Figure 12. Margins provided by ANN-1 and ANN-2.

fire classification. Because of this fact, tunnel width was not considered as input for the belt fire classification model. This result agrees with results obtained by Li and Ingason[40] in which it was concluded that for large fires, the critical velocity is independent of tunnel width.

In order to define the effect of belt position and tunnel height when combined with air velocity on fire classification, 2D margins were determined. Probability estimates of 1000 scenarios inside of the intervals of air velocity and belt position, and air velocity and tunnel height were calculated using ANN-1 and ANN-2, respectively. Scenarios with probabilities equal to 0.5 were assumed to be on the margins. Margins provided by ANN-1 and ANN-2 are shown in Figure 12, respectively. It is worth of mentioning that the 0.5 probability points provided by ANN-1 and ANN-2 were fitted to linear trendlines.

The equation of margin provided by ANN-1 with an R-squared of 1.0 is shown in equation (11). This margin indicates that as belt position decreases, longitudinal air velocity must be greater in order that fires are classified as Type I. In other words, the lower is the distance between the mine roof and conveyor belt surface, the higher must be the air velocity in order to avoid that tenability limits are exceeded due to the presence of rollback. This fact can be attributed to the radiation of heat to the belt surface. With lower surface to roof distance, roof would have a higher temperature and would radiate more heat back increasing belt burning rate, fire size, and fire buoyancy force which could increase the amount of smoke upwind from the fire when inertial forces generated by ventilation are not high enough. This

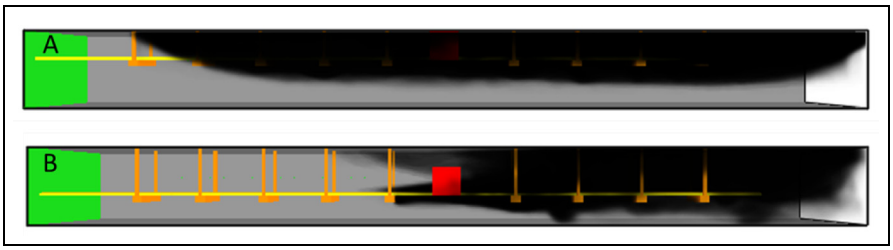

Figure 13. Smoke in Scenarios A and B after the onset of the flame spread.

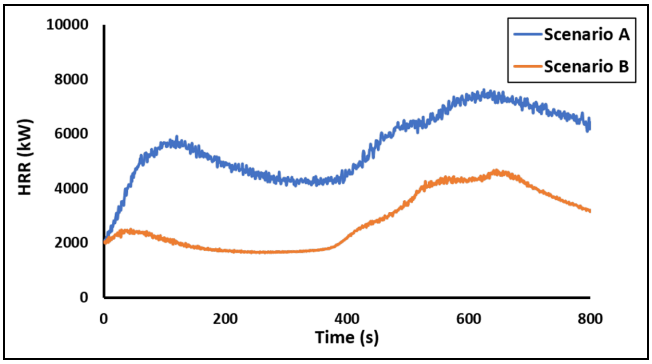

Figure 14. HRR for Scenarios A and B.

explanation agrees with a study carried out by Yuan et al.,[25] in which it was found that for lower surface-to-roof distances, the flame spread rate was greater, and conditions for fire development and growth were better due to more heat radiation from roof and belt. In addition, small separations between the roof and belt surface limit the accessibility of oxygen to the flame leading to a combustion within the fuel-rich region where more rapid flames and high smoke production are observed[25]

$$\mathrm{BP} = -2.04V + 4.69 \tag{11}$$

$$H = 1.99V - 1.35 \tag{12}$$

In the above equations, BP is the belt position (m), V is the air velocity (m/s), and H is the tunnel height (m).

To visualize the effects of belt position on fire classification and fire intensity, simulation results of smoke layer and HRR for two scenarios named as A and B are shown in Figures 13 and 14, respectively. Both scenarios have the same air velocity and tunnel height, but different belt position as shown in Table 11. For Scenario A, it can be seen the presence of roll-back leading to a non-tenable scenario classified as Type II. Figure 14 shows the maximum fire size and fire size values over time are greater in Scenario A than in Scenario B due to the proximity of the belt surface to the roof. In Scenario A, the buoyancy force generated by a larger fire overcomes the inertial forces generated by the ventilation with an air velocity of

Table 11. Input parameters for Scenarios A and B.

Scenario	A	B
Air velocity (m/s)	1.8	1.8
Tunnel height (m)	2.4	2.4
Belt position (m)	0.8	1.4

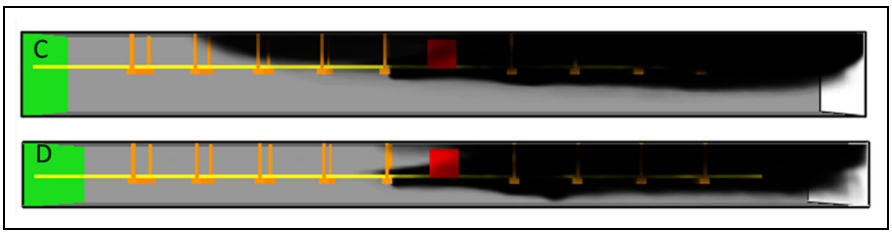

Figure 15. Smoke in Scenarios C and D after 600 s of the onset of the flame spread.

Table 12. Input parameters for Scenarios A and B.

Scenario	C	D
Air velocity (m/s)	2.0	2.0
Tunnel height (m)	2.6	2.0
Belt position (m)	1.0	1.0

1.8 m/s. On the contrary, in Scenario B, the ventilation is able to keep the smoke away upwind from the fire due to a smaller fire size being classified as a scenario Type I.

The equation of margin provided by ANN-2 with an R-squared of 1.0 is shown in equation (12). This margin shows that as tunnel height increases, air velocity must be greater for fire scenarios to be classified as Type I as shown in Figure 12. This turns out that the longitudinal air velocity must be greater for taller tunnel heights in order to avoid rollback. This result agrees with a study carried out by Li and Ingason,[40] in which it was found that the critical velocity considerably rises as tunnel height increases. The influence of tunnel height on fire classification and fire intensity can be seen when Scenarios C and D are compared. Parameters of Scenarios C and D are shown in Table 12. Rollback is seen for Scenario C with greater tunnel height while for Scenario D, there is not smoke upwind from the fire, as shown in Figure 15. HRR for Scenarios C and D is shown in Figure 16. As was seen for belt position analysis, tunnel height also impacts the HRR peak and the belt burning rate of the conveyor. For Scenario C, it can be seen a higher HRR peak producing a high amount of smoke that cannot be kept away upwind from the fire.

For the determination of the belt conveyor belt fire classification model as well as its accuracy, the data set was split into two. 90% which was used to select the architecture and train

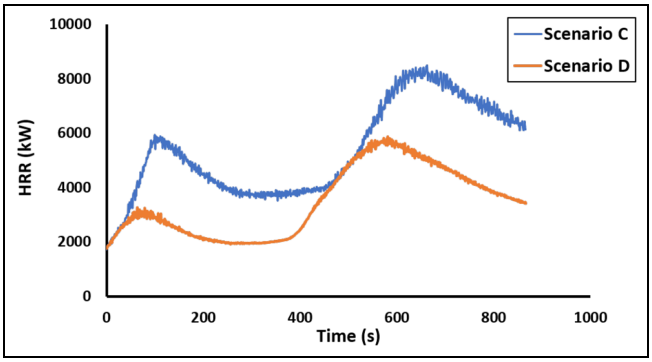

Figure 16. HRR for Scenarios C and D.

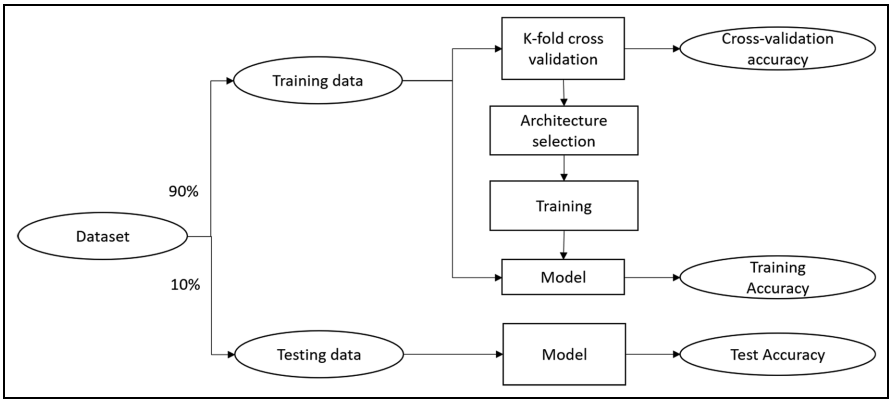

Figure 17. Methodology for model determination.

the ANN. The remaining 10% was used as testing data set. The architectures shown in Table 9 were tested to select the best architecture for ANN-4 through threefold CV. Then, ANN-4 was trained using training data set to determine the model and training accuracy. L2-norm regularization was also used during training of ANN-4. Finally, the model was tested using the test data set with the objective of determining test accuracy of the model. A schematic showing a general view of the methodology for model determination is shown in Figure 17.

As indicated previously, air velocity, belt position, and tunnel height parameters were used as input parameters for model determination. As shown in Table 13, training and test accuracies of 96.30% and 95.0% were obtained for ANN-4, respectively. This accuracy indicates the capability of the model of predicting 95 scenarios correctly out of 100 unseen scenarios. Following the same procedure for the determination of previous margin equations, points with estimate probabilities of 0.5 were obtained to determine the plane corresponding to the margin. Equation of the plane is shown in equation (13). The R-squared of the plane equation was 1.0

$$0.80V + 0.28\mathrm{BP} - 0.35H = 1 \tag{13}$$

Table 13. ANN-4 architecture and accuracy.

Name	Architecture	CV accuracy (%)	Training accuracy (%)	Test accuracy (%)
ANN-4	Arch3	96.01	96.30	95.0

Conclusion

A model was developed to classify conveyor belt fires to determine the most adequate firefighting strategy. In addition, the effects of design parameters such as belt position and mine entry dimensions on the fire classification were analyzed. This study was achieved using a methodology that consists of CFD simulations and ANNs. CFD simulations were used to predict the effects of fires spreading over conveyor belts. To predict realistic results, parameters used in CFD simulations were calibrated and CFD results were validated with experimental test results available in the literature. ANNs were used for the determination of parameter effects on fires outcome and the model for conveyor belt fire classification.

Validation and calibration results demonstrated that Yuan et al.'s[10] approach can predict real belt fire conditions with certain degree of certainty, despite the flame spread phenomenon is not solved completely due to the lack of physics in the model. In the model obtained using this approach, SBR was modeled as a single material component with reference rate and reference temperature of 0.0022 s^{-1} and 368°C, respectively. However, the results of effects of design parameters on fire classification indicate that scenarios with closer belt positions to the roof and taller tunnel heights require a higher air velocity to be classified as Type I. Also, it was found that tunnel width has a negligible influence on the conditions at the attack position as well as on the fire classification. Besides, the critical velocity for mine conveyor belt fire scenarios simulated in this study was estimated between 1.7 and 2.2 m/s. When air velocity, belt position, and tunnel height were used as the input parameters, the conveyor belt fire classification model had accuracies of 96.30% and 95.00% for training and testing data set, respectively.

In addition to the determination of the design parameter effects on the fire classification, the margin classification model equation provides an approximation of the critical velocity for mine belt entries based on design parameters such as belt position and tunnel height. It can be said that methodology used in this study can be applied for fire classification on different mine fire locations contributing to better mine fire emergency plans. Future work should be focused on improving the modeling of ignition and pyrolysis processes of SBR as well as on formalizing the firefighters' exposure limits in underground mining. Also, future studies can address the determination of response time (i.e. approach time) that is defined as the time first responders and fire brigade members have to approach and start attacking the fire once the CO alarms are activated before at least one of the tenability limits is exceeded.

Declaration of conflicting interests

The author(s) declare that they have no known competing financial interests or personal relationships that could have appeared to influence the work reported in this paper.

Funding

The author(s) disclosed receipt of the following financial support for the research, authorship, and/or publication of this article: This research was supported by the Contract No. 200-2014-59669, awarded by the National Institute for Occupational Safety and Health (NIOSH). The findings and conclusions in this report are those of the authors and do not reflect the official policies of the Department of Health and Human Services nor does mention of trade names, commercial practices, or organizations imply endorsement by the US Government.

ORCID iD


Manuel J Barros-Daza https://orcid.org/0000-0003-1109-3524

References

1. Conti RS, Chasko LL, Wiehagen WJ, et al. An underground coal mine fire preparedness and response checklist: the instrument. Technical report, National Institute for Occupational Safety and Health (NIOSH), Pittsburgh, PA, 2000.
2. Conti RS, Chasko LL, Wiehagen WJ, et al. Fire response preparedness for underground mines. Technical report, National Institute for Occupational Safety and Health (NIOSH), Pittsburgh, PA, 2005.
3. National Fire Protection Association (NFPA). *NFPA glossary of terms. Technical report*. NFPA, 2021, https://www.nfpa.org/Codes-and-Standards/Resources/Glossary-of-Terms
4. Forbes J and Grove W. Procedure in sealing and unsealing mine fires and in recovery operations following mine explosions. *Technical report, United States Department of the Interior, Washington, DC*, 1938, https://digital.library.unt.edu/ark:/67531/metadc40317/m2/1/high_res_d/bomminerscirc_36_w.pdf
5. Litton CD, Lazzara CP and Perzak FJ. Fire detection for conveyor belt entries. *Technical report, United States Department of the Interior, Washington, DC*, 1991.
6. Perera IE and Litton CD. Impact of air velocity on the detection of fires in conveyor belt haulageways. *Fire Technol* 2011; 48(2): 405–418.
7. Kim HK, Lönnermark A and Ingason H. *Effective firefighting operations in road tunnels*. Borås: SP Technical Research Institute of Sweden, 2010.
8. US Code of Federal Regulations. CFR, title 30 (mineral resources) part 75. *Mandatory safety standards—underground coal mines*, 2016, https://www.msha.gov/regulations/standards-regulations
9. McGrattan K, Hostikka S, Floyd J, et al. *Fire dynamics simulator user's guide*, vol. 1019, 6th ed. Gaithersburg, MD: National Institute of Standards and Technology, 2016. DOI: 10.6028/NIST.SP.1019.
10. Yuan L, Mainiero RJ, Rowland JH, et al. Numerical and experimental study on flame spread over conveyor belts in a large-scale tunnel. *J Loss Prevent Proc* 2014; 30: 55–62.
11. Edwards JC and Hwang CC. CFD modeling of fire spread along combustibles in a mine entry. In: *SME annual meeting and exhibit*, pp. 4–8, https://www.cdc.gov/niosh/mining%5C/UserFiles/works/pdfs/cmofs.pdf
12. Lowndes IS, Silvester SA, Giddings D, et al. The computational modelling of flame spread along a conveyor belt. *Fire Safety J* 2007; 42(1): 51–67.
13. Lazzara C and Perzak F. Effect of ventilation on conveyor belt fires. In: *Proceedings of symposium on safety in coal mining*, Pretoria, South Africa, October 1987.
14. Rowland J and Smith AC. *Flammability of wider conveyor belts using large-scale fire tests 2007*. 2006, https://www.cdc.gov/niosh/mining/UserFiles/works/pdfs/fowcbu.pdf
15. Haghighat A and Luxbacher K. Tenability analysis for improvement of firefighters' performance in a methane fire event at a coal mine working face. *J Fire Sci* 2018; 36(3): 256–274.
16. Goodfellow I, Bengio Y and Courville A. Deep learning, 2016, http://www.deeplearningbook.org
17. Hodges JL, Lattimer BY and Luxbacher KD. Compartment fire predictions using transpose convolutional neural networks. *Fire Safety J* 2019; 108: 102854.
18. McGrattan K, Hostikka S, Floyd J, et al. Fire dynamics simulator (Version 6), technical reference guide. *NIST—Special Publication*, 2018, http://www.ncbi.nlm.nih.gov/pubmed/8409852
19. ICIS. Styrene-Butadiene Rubber (SBR) uses and outlook—ICIS Explore, 2010, https://www.icis.com/explore/resources/news/2007/11/06/9076467/styrene-butadiene-rubber-sbr-uses-and-outlook/
20. Grieco E, Bernardi M and Baldi G. Styrene–butadiene rubber pyrolysis: products, kinetics, modelling. *J Anal Appl Pyrol* 2008; 82: 304–311.
21. Lin JP and Chang CY. Pyrolytic treatment of rubber waste: pyrolysis kinetics of styrene-butadiene rubber. *J Chem Technol Biot* 1996; 66: 7–14.
22. Tewarson A. Generation of heat and chemical compounds in fires. In: DiNenno PJ (ed.) *SFPE handbook of fire protection engineering*. 3rd ed. 2002, pp. Section 3–111, https://www.globalspec.com/reference/76878/203279/chapter-4-generation-of-heat-and-chemical-compounds-in-fires
23. Wiberg K and Fenoglio R. Heats of formation of C_4H_6 hydrocarbons. *J Am Chem Soc* 1968; 90: 3395–3397.
24. Tewarson A, Jiang FH and Morikawa T. Ventilation-controlled combustion of polymers. *Combust Flame* 1993; 169: 151–169.
25. Yuan L and Litton CD. *Experimental study of flame spread on conveyor belts in a small-scale tunnel*. Pittsburgh, PA: National Institute for Occupational Safety and Health, 2007.
26. Li YZ, Vylund L, Ingason H, et al. Influence of fire suppression on combustion products in tunnel fires. *Fire Safety J* 2018; 97: 96–110.
27. Lyon R. Plastics and rubber. In: Harper CA (ed.) *Handbook of building materials for fire protection*. New York: McGraw Hill Professional, 2004, pp. 3.1–3.46.

28. Singer J Philip and Tye R. *Thermal, mechanical, and physical properties of selected bituminous coals and cokes*. Pittsburgh, PA: Bureau of Mines, 1979.
29. Gissi E. An introduction to fire simulation with FDS and Smokeview. *October* 2009; 164, http://creativecommons.org/licenses/by-sa/3.0/
30. Fernandez Pello A. Flame spread modeling. *Combust Sci Technol* 1984; 39: 1–6.
31. NFPA. NFPA 502: Standard for road tunnels, bridges, and other limited access highways. 2020, https://www.nfpa.org/codes-and-standards/all-codes-and-standards/list-of-codes-and-standards/detail?code = 502
32. Gehandler J, Ingason H, Lönnermark A, et al. *Performance-based requirements and recommendations for fire safety in road tunnels (FKR-BV12)*. SP Technical Research Institute of Sweden, 2013.
33. Ingason H, Li YZ and Lönnermark A. Tunnel fire ventilation. In: Ingason H, Li YZ and Lönnermark A (eds) *Tunnel fire dynamics*, vol. 53. New York: Springer, 2015, pp. 333–360, http://link.springer.com/10.1007/978-1-4939-2199-7
34. Fridolf K, Andree K, Nilsson D, et al. The impact of smoke on walking speed. *Fire Mater* 2014; 38(7): 744–759.
35. Scikit-learn. Neural network models (supervised)—scikit-learn 0.24.1 documentation, 2020, https://scikit-learn.org/stable/modules/neural_networks_supervised.html
36. Mcpherson MJ. Part 5: Fires and Explosions. In: Mine Ventilation Services Inc. (ed.) *Subsurfaceventilation engineering*. 1st ed, chapter 21. Mine Ventilation Services Inc., 1993, pp. 11–15.
37. Thomas PH. *The movement of buoyant fluid against a stream and the venting of underground fires*. Fire research note no. 351. Watford: Fire Research Station, 1958.
38. Thomas PH. *The movement of smoke in horizontal passages against an air flow*. Fire research note no. 723. Watford: Fire Research Station, 1968.
39. Danziger N and Kennedy W. Longitudinal ventilation analysis for the Glenwood Canyon tunnels. In: *Proceedings of the fourth international symposium on the aerodynamics ventilation of vehicle tunnels*, York, March 1982, pp. 169–186, https://scirp.org/reference/referencespapers.aspx?referenceid = 120230
40. Li YZ and Ingason H. Effect of cross section on critical velocity in longitudinally ventilated tunnel fires. *Fire Safety J* 2017; 91: 303–311.

Author biographies

Manuel Barros-Daza is a PhD candidate in the Mining and Minerals Engineering Department at Virginia Tech. His research areas are mine ventilation, computational modeling, mine ventilation, machine learning, and fire dynamics.

Dr. Kray Luxbacher is a professor and associate department head of Mining and Minerals Engineering Department at Virginia Tech. Her research areas are mine ventilation and mine health and safety.

Dr. Brian Lattimer is a professor of Department of Mechanical Engineering at Virginia Tech. His research areas are thermal-fluid sciences, reacting flows and fire dynamics, material high temperature behavior, firefighting automation, technology, and suppression.

Dr. Jonathan Hodges is a service line leader in advanced modeling at Jensen Hughes. His research areas are computational modeling, data analytics, machine learning, computer vision, robotics, and fire dynamics.